

# Centrifugal melt spinning of polyvinylpyrrolidone (PVP)/triacontene copolymer fibres

Tom O'Haire<sup>1,\*</sup>, Stephen. J. Russell<sup>1</sup>, and Christopher M. Carr<sup>1</sup>

<sup>1</sup> School of Design, University of Leeds, Leeds LS2 9JT, UK

Received: 21 January 2016

Accepted: 2 May 2016

© The Author(s) 2016. This article is published with open access at Springerlink.com

## ABSTRACT

Polyvinylpyrrolidone/1-triacontene (PVP/TA) copolymer fibre webs produced by centrifugal melt spinning were studied to determine the influence of jet rotation speed on morphology and internal structure as well as their potential utility as adsorbent capture media for disperse dye effluents. Fibres were produced at 72 °C with jet head rotation speeds from 7000 to 15,000 r min<sup>-1</sup>. The fibres were characterised by means of SEM, XRD and DSC. Adsorption behaviour was investigated by means of an isothermal bottle point adsorption study using a commercial disperse dye, Dianix AC-E. Through centrifugal spinning nanofibers and microfibers could be produced with individual fibres as fine as 200–300 nm and mean fibre diameters of ca. 1–2 μm. The PVP/TA fibres were mechanically brittle with characteristic brittle tensile fracture regions observed at the fibre ends. DSC and XRD analyses suggested that this brittleness was linked to the graft chain crystallisation where the PVP/TA was in the form of a radial brush copolymer. In this structure, the triacontene branches interlock and form small lateral crystals around an amorphous backbone. As an adsorbent, the PVP/TA fibres were found to adsorb 35.4 mg g<sup>-1</sup> compared to a benchmark figure of 30.0 mg g<sup>-1</sup> for a granular-activated carbon adsorbent under the same application conditions. PVP/TA is highly hydrophobic and adsorbs disperse dyes through the strong “hydrophobic bonding” interaction. Such fibrous assemblies may have applications in the targeted adsorption and separation of non-polar species from aqueous or polar environments.

## Introduction

The ability to influence the interaction between multi-component liquids and fibre surfaces to control behaviour such as mutual hydrophobicity and oleophilicity is important in numerous applications such as filter media, chemical sorbents and protective

clothing. An attractive development strategy is to identify novel polymer systems for fibre production for use in such products. However, the limitations and difficulties when processing such polymers on conventional spinning lines continue to restrict feasibility. Polyvinylpyrrolidone/1-triacontene (PVP/TA) consists of a polyvinylpyrrolidone (PVP)

Address correspondence to E-mail: t.ohaire@leeds.ac.uk

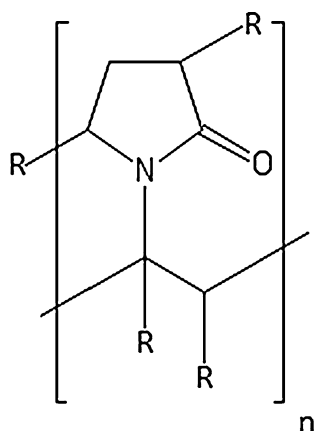


**Figure 1** Typical structure of alkyated PVP brush copolymers, where R is either hydrogen or a long chain hydrocarbon such as  $C_{30}H_{61}$  in the case of PVP/TA [1, 2].

backbone with 1-triacontene ( $C_{30}$ ) side chains [1], Fig. 1, and whilst homogenous PVP is hydrophilic and water soluble, PVP/TA is non-polar and highly hydrophobic. The 1-triacontene is densely grafted and forms a brush copolymer structure [2] and in this form, the inherent hydrophilicity of the PVP is modified by the hydrophobicity of the non-polar  $C_{30}$  chains [3, 4]. Currently, PVP/TA is used as a waterproofing agent in cosmetics and sunscreens as well as in printing inks and other liquid formulations [1, 4–7]. It is normally used as a film or in the form of a liquid dispersion. Given the hydrophobicity, water insolubility and oleophilic behaviour of PVP/TA, the production of fibres from this copolymer provides significant opportunities to extend the range of industrial applications.

Spinning of homogenous PVP homopolymer and in blends with other polymers has been previously demonstrated through electrospinning [8, 9] and needleless centrifugal spinning [10]. Fibres have been formed using PVP dissolved in volatile solvents in conjunction with: a  $CO_2$  atmosphere [9]; a saline sheath [8]; and through centrifugal electrospinning, a hybrid technique [11]. The needleless centrifugal spinning of PVP used a 20 % aqueous solution to form fibres as  $400 \pm 100$  nm in diameter at  $4000 \text{ r min}^{-1}$ . However, there is little information on the melt processing of PVP into fibres [12] or the utilisation of PVP/TA or similar alkyated PVP materials in fibre spinning studies. Although electrospinning is a versatile spinning technique, it is limited by many factors such as the need to form an

electrified jet. PVP/TA is insoluble in aqueous solvents and has a depressed melting point compared to PVP, creating the possibility of low temperature melt processing. Recently, centrifugal spinning has been increasingly applied to form non-ideal materials into ultrafine fibres from either polymer melts or solutions [13]. This technique involves rotating polymer fluids at high speeds to induce jet formation and elongation without the need for external drawing, electrostatic forces or high velocity hot air [14]. It has been demonstrated that centrifugal spinning can readily produce fibres finer than  $1 \mu\text{m}$  from a variety of polymer materials [14, 15] from either thermoplastic liquid melts or solutions. Fibres have been produced from conventional thermoplastics such as nylon and polyester; speciality polymers such as polycaprolactone and poly(lactic acid); bismuth; ceramic materials; compounds of polypropylene and carbon nanotubes; compounds of poly(ethylene terephthalate) with graphene [13, 16, 17]. In centrifugal spinning, the operating conditions can have a significant influence on fibre diameter and investigation is often necessary to establish optimum parameters, balancing fibre fineness and the level of beading [15].

Forming PVP/TA into submicron fibres using centrifugal spinning has the potential to significantly increase the available surface area of the material compared to films or granulate. This would usefully facilitate the “capture” of molecules through mutual hydrophobic and oleophilic adsorption [4, 18]. Specifically, this could assist in the chemical adsorption of hydrophobic disperse dyes from textile waste effluent with improved efficiency compared to traditional sorbents. Disperse dyes are used in the colouration of polyester and other synthetic fibres and are typically non-polar and hydrophobic. Disperse dyes are not always decolourised or decomposed by biological or reductive treatments and may therefore persist in the environment and in aquatic systems [19, 20]. Adsorption of disperse dyes on to a capture media has been proposed as one solution for removal, possible recycling and minimising potential accumulation in the environment [21]. In addition to the treatment of dyehouse effluent, such hydrophobic/oleophilic fibres could also be used as sorbents and capture agents in domestic laundering, potentially preventing the unwanted cross-staining of dyes [22].

The purpose of this investigation was to study the centrifugal spinning of submicron PVP/TA

copolymer fibres and to evaluate the structure and physical properties of resulting fibres and fabrics. In addition to studying as-spun fibre morphology by scanning electron microscopy (SEM), the thermal behaviour and fine structure of the fibres were elucidated by differential scanning calorimetry (DSC) and X-ray diffraction (XRD), respectively. Finally, the potential applications of PVP/TA fibre in porous sorption media were explored by comparing the adsorption of a disperse dye against an activated carbon benchmark.

## Materials and methods

### Materials

The polyvinylpyrrolidone/1-triacontene polymer was supplied as a flake by Sigma Aldrich, UK, under the commercial name Antaron WP660, which is also known as triacontyl polyvinylpyrrolidone, CAS registered as 2-pyrrolidinone, 1-ethenyl with 1-triacontene (CAS number 136,445-69-7). A commercial anthraquinone-based disperse dye (Dianix Blue AC-E, CAS number 98725-74-7) was supplied by Dystar Textilfarben, Germany, and was used without further treatment or purification. Chromatography grade acetone, (>99.8 %) and laboratory grade Triton X100 (CAS 9002-93-1), both via Sigma Aldrich, UK, were used for the dye adsorption study along with an activated carbon adsorbent, 1 mm granular Norit<sup>®</sup> supplied by Sigma Aldrich, UK. The as-delivered activated carbon was rinsed in deionised water and then dried at 50 °C for 24 h in a laboratory oven prior to use.

### Capillary rheometry

Apparent melt viscosity of PVP/TA was assessed using a RH2000 capillary rheometer (Bohlin Instruments, UK) configured with a capillary die 1 mm in diameter and 16 mm in length. Rheology measurement was conducted at temperatures of 65, 70, 75, and 80 °C with piston speeds of 50, 70, and 120 mm min<sup>-1</sup>.

### Centrifugal spinning

Fibre production was carried out using the Force-spinning<sup>™</sup> L1000 M centrifugal spinner (Fiberio,

USA) in a melt spinning configuration using tri-orifice spinnerets with two different orifice diameters available: 159 µm (fine) and 602 µm (coarse). A static arrangement of posts positioned 115 mm circumferentially from the spinneret was used as a supporting collector. The influence of rotational speed was assessed by varying the rotational speed from 6000 to 15,000 r min<sup>-1</sup>. A mass of 300 mg of PVP/TA was added to the spinneret and external heat was applied until a stable polymer temperature of 72 ± 1 °C was achieved. The spinneret was then accelerated and held constant at a given speed for 45 s before decelerating. A minimum of two fibrous webs was formed at each operating condition for assessment. For the dye adsorption investigations, the PVP/TA fibres were produced at a rotational speed of PVP/TA at 11,000 r min<sup>-1</sup> using the coarser spinneret (602 µm) only.

### Scanning electron microscopy (SEM) analysis

The fibres were examined using a Jeol JSM-6610LV scanning electron microscope (Japan). The fibrous samples were mounted on conductive carbon tape and gold sputter coated prior to analysis. An acceleration voltage of 5–15 kV was used with a typical working distance of 100 mm. Images were captured at magnifications of ×1000 for fibre diameter measurements. Higher magnifications were used to image specific areas and fibres of interest. Image analysis software, Image J, was used to assess the average fibre diameters by evaluating a minimum of 200 fibres from 5 different regions of the sample stub.

### Thermal analysis

The thermal properties of the PVP/TA fibres and flake were assessed using a Perkin Elmer Jade differential scanning calorimeter. Samples were analysed in aluminium pans from –10 to 250 °C at a rate of 20 °C min<sup>-1</sup> with a nitrogen gas supply of 20 mL min<sup>-1</sup>. A heat-cool-heat cycle was conducted on a fibrous sample from 25 to 120 °C at the same heating/cooling rate under identical conditions.

### X-ray diffraction (XRD) analysis

The internal fine structure of the PVP/TA raw material and as-spun PVP/TA fibres were

investigated using a PANalytical X'Pert MPD X-ray diffractometer. The as-supplied PVP/TA flake was analysed without modification and the fibrous webs were cold pressed flat into a thin sample prior to observation. The radiation source was  $\text{CuK}\alpha$  ( $\lambda = 1.540 \text{ \AA}$ ) and the scans were taken in the theta:theta orientation through  $4^\circ$ – $60^\circ$  with a step size of  $0.066^\circ$ .

## Dye adsorption study

The level of dye removal by the fibres and the subsequent adsorption isotherm for the PVP/TA fibres and the disperse dye were determined using a bottle point adsorption method [23, 24]. Dye dispersions of concentrations of  $25$ – $300 \text{ mg dm}^{-3}$  were made using Dianix Blue AC-E and distilled water. The PVP/TA fibres were added to the dispersions at a ratio of  $0.5 \text{ g}$  adsorbent to  $0.1 \text{ dm}^3$  of liquor. Triton X100 was added at a concentration of  $1 \text{ g dm}^{-3}$  to act as a wetting agent. A parallel set of dispersions were treated with granulated activated carbon under the same conditions. The dispersions were stirred for 3 days in a sealed jar using a magnetic impeller. After this period, the dye liquors were passed through porosity 2 sintered glass crucibles to separate the PVP/TA fibres and carbon granules from the solutions. The filtrates were mixed 50:50 with HPLC grade acetone in order to dissolve the disperse dye molecules and the  $\lambda_{\text{max}}$  was measured using UV-Vis spectrophotometry. The measured values then converted into concentrations using a calibration chart produced for Dianix Blue AC-E in 50:50 distilled water and acetone.

## Results and discussion

### Capillary rheometry

The capillary rheometry results given in Fig. 2 show that the melt viscosity of PVP/TA is sensitive to temperature changes, reducing from  $>25 \text{ Pa s}^{-1}$  at temperatures  $65$  and  $70^\circ \text{C}$  to  $<2 \text{ Pa s}^{-1}$  at  $80^\circ \text{C}$ .

### Centrifugal spinning of PVP/TA

PVP/TA was successfully formed into fibrous webs using melt-centrifugal spinning using both the coarse and fine spinnerets at a polymer temperature of

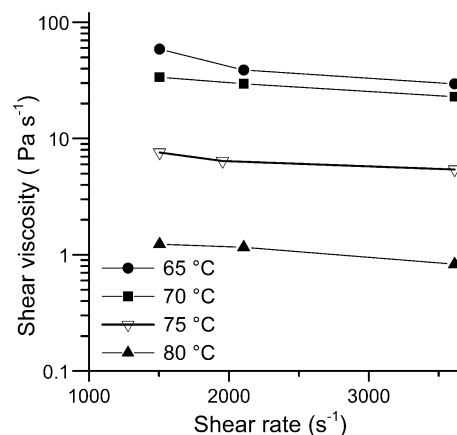


**Figure 2** Apparent shear viscosity curves as a function of shear rate and temperature.

$72 \pm 1^\circ \text{C}$ . When using the fine melt spinneret, fibres were successfully formed at all rotational spinneret speeds from  $12,000$  to  $15,000 \text{ r min}^{-1}$  with all other conditions fixed. At  $11,000 \text{ r min}^{-1}$  and below, the PVP/TA melt was unable to be ejected from the fine spinneret due to the relatively high melt viscosity. It is proposed that at low rotational speeds the inertia of the melt is insufficient to overcome the capillary resistance of the  $159 \mu\text{m}$  orifice; thus, the critical speed necessary for successful extrusion was in excess of  $11,000 \text{ r min}^{-1}$  for the combination of spinneret and temperature investigated [25]. At  $16,000 \text{ r min}^{-1}$  and above the level of beading it became excessive and the level of fibre produced decreased significantly. It is proposed that the inertial and aerodynamic forces encountered at such rotational speeds is excessively high, leading to jet break-up and bead formation as instabilities become critical [25, 26]. For the coarse spinneret ( $602 \mu\text{m}$ ), the critical rotational speed was lower, with fibres being produced at speeds  $7000 \text{ r min}^{-1}$  and above. This was due to coarser spinneret requiring a lower inertial pressure to overcome the capillary resistance. With this spinneret, the beading became excessive at  $15,000 \text{ r min}^{-1}$ .

Figure 3 shows SEM micrographs from selected webs which show that the PVP/TA fibres produced were cylindrical and smooth with very little surface texture. A disparity in fibre diameters within a sample can also be observed. Variation in fibre diameter was evident with very fine fibres ( $>300 \text{ nm}$ ) proximal with much coarser fibres ( $<5 \mu\text{m}$ ), resulting in a relatively high value of standard deviation, Table 1. A

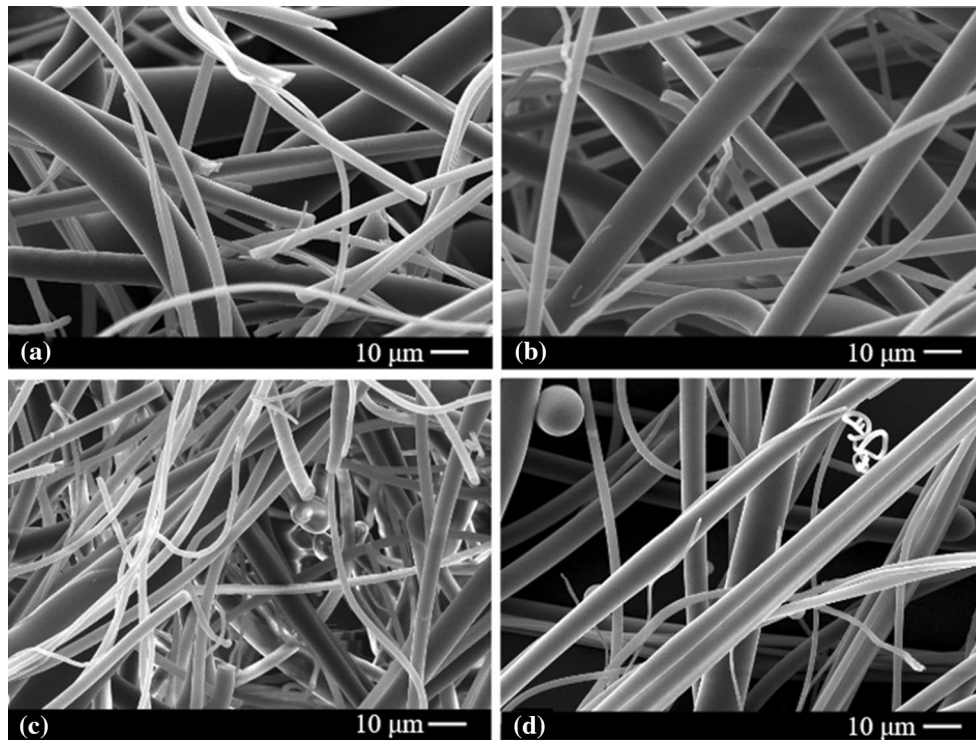


**Figure 3** SEM micrographs of PVP/TA fibres produced using the coarse spinneret at **a** 8000, **b** 10,000, **c** 12,000 and **d** 14,000 r min<sup>-1</sup>, respectively.

**Table 1** Mean fibre diameters for PVP/TA fibres made through centrifugal spinning

Spinneret	Fibre diameter (µm)	Rotational speed (r min <sup>-1</sup> )										
		6000	7000	8000	9000	10,000	11,000	12,000	13,000	14,000	15,000	16,000
Coarse	$\bar{x}$	x	7.88	5.02	5.38	4.23	4.01	3.43	2.81	2.33	b	x/b
	$\sigma$	x	6.16	3.12	4.31	3.04	3.00	2.20	1.69	1.47	b	x/b
Fine	$\bar{x}$	x	x	x	x	x	x	1.83	1.43	1.52	1.46	b
	$\sigma$	x	x	x	x	x	x	1.66	1.02	1.20	0.87	b

*x* web was not produced, *b* excessive beading/spraying occurred

one-way ANOVA ( $\alpha = 0.05$ ) analysis of the data on the centrifugal revealed that the means were statistically different for conditions measured [ $p < 0.001$ ;  $F(63.1) > F_{crit}(1.79)$ ] and different within the samples formed using the coarse spinneret [ $p < 0.001$ ;  $F(23.6) > F_{crit}(2.02)$ ] and the fine spinneret [ $p < 0.05$ ;  $F(4.29) > F_{crit}(2.61)$ ].

The formation of coarse fibres was attributed to the acceleration and deceleration phases in the spinning cycle; the turbulent attenuation of fibres; premature jet breakage; and variability in the throughput of

polymer. It is proposed that a combination of these factors contributes to generating fibres with a range of fibre diameters significantly greater than the reported mean value. It has been previously reported that mean fibre diameter of centrifugal spun fibres decreases with spinning duration and it is proposed that a continuous machine would create a lower proportion of coarse fibres as the effects of acceleration and deceleration are minimised [15].

At low spinneret rotation speeds, the extensional forces on the polymer jet are lower relative to higher

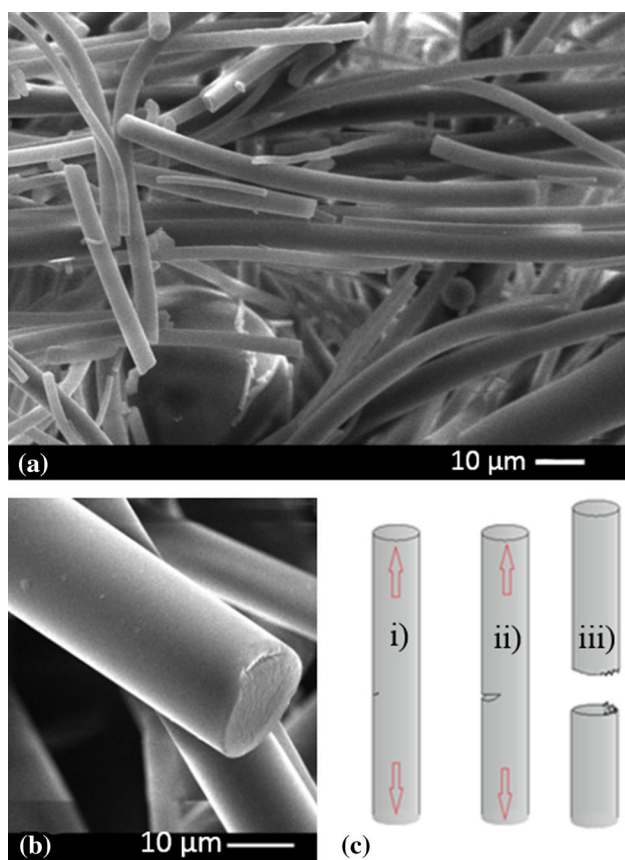


**Figure 4** Fibre end breaks as observed in PVP/TA fibres formed in **a** 15,000 rpm (fine spinneret); **b** 12,000 r min<sup>-1</sup> (coarse spinneret) with the mechanism of brittle fracture modelled in **c**.

speeds and the level of attenuation is lower, resulting in larger fibre diameters. As with many polymers, the formation of PVP/TA into fibres is a balancing act between polymer throughput, initial jet diameter, jet attenuation and jet break-up [25, 26].

Examination of the discontinuities or fibre ends resulting from breakage is shown in Fig. 4a, b, which shows that the fibre end breaks are relatively abrupt and smooth-faced with no indications of fibrillation or ductile fracture. Such fibre breakage was observed across all samples irrespective of the process conditions employed, and therefore appears to be a characteristic feature of centrifugally spun PVP/TA fibres and the bulk properties of the co-polymer. A slight imperfection frequently observed on one edge of the break cross section is strongly indicative of brittle tensile fracture, as previously detailed [27].

A schematic representation of the brittle tensile fracture in a PVP/TA fibre is shown in Fig. 4c. Within a fibre with a surface flaw (i), the crack will

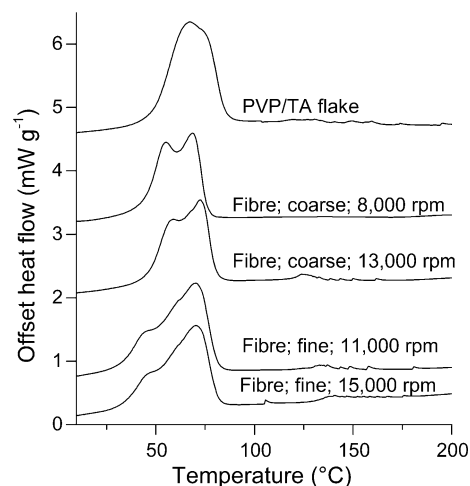


**Figure 5** DSC thermograms of PVP/TA fibres formed using both the coarse and fine spinnerets at selected processing speeds.

propagate (ii) until eventually the fibre breaks (iii) leaving a characteristic clean break across most of the width of the fibre fracture face. The increased propensity of fibre breakage is not only thought to be a combination of disruption of polymer streams during spinning but also to fracture of fibres during handling of the PVP/TA webs, which although self-supporting, were relatively weak. Bending failure in brittle materials also produces the clean fracture as shown in Fig. 4 [28], and it is likely that load in bending also causes a significant number of breaks.

### Internal fine structure and thermal analyses of fibres

The DSC experiments revealed the thermal behaviour of PVP/TA flake and fibres when heated through the melting point, Fig. 5.

The PVP/TA flake has a broad melting endotherm with  $T_{\text{onset}}$  at 55 °C and a  $T_{\text{melt}}$  at 72 °C with a profile typical of the melting of a semicrystalline polymer with one crystal form. The DSC thermograms of the PVP/TA fibres exhibit a significantly different thermal profile. The fibre endotherms have a double peak or shoulder trace (50–60 °C), which is most clearly evident in the fibres produced from the coarse spinneret. This double endotherm indicates that PVP/TA fibres have a clear  $\alpha$  and  $\beta$  peak profile not observed in the flake. The major  $\alpha$  peak was the main melt transition and is found at around 76–80 °C which was preceded by smaller  $\beta$  peak at 57–62 °C that

represented a pre-melt transition. Double melting peaks such as these in DSC can be attributed to the following conditions:

- i. Two distinct crystal morphologies and configurations;
- ii. Re-crystallisation behaviour during the DSC scan [29];
- iii. Material is actually a binary blend of two different grade products [30];

A typical heat-cool-heat DSC scan for PVP/TA is given in Fig. 6 which shows that the double peak profile observed in fibres was erased by the first heating cycle and the melting profile for the second heat scan does not include this secondary peak. This secondary heating profile was observed in all the PVP/TA fibres regardless of processing conditions. The deletion of this early peak indicates that it is a feature of processing not inherent to PVP/TA. The absence of such a  $\beta$ -peak for the flake material suggests that conditions (i) and (ii) are not applicable in PVP/TA. It is thus concluded and appears that centrifugally spun PVP/TA has two crystal conformations: a primary  $\alpha$ -crystal that is found in both the flake and the fibre; and a secondary  $\beta$ -crystal form, which melts at a lower temperature and is formed during the processing of PVP/TA into a fibre using melt processing.

The XRD patterns, Fig. 7, for PVP/TA flake and the centrifugally spun fibres generated two dominant

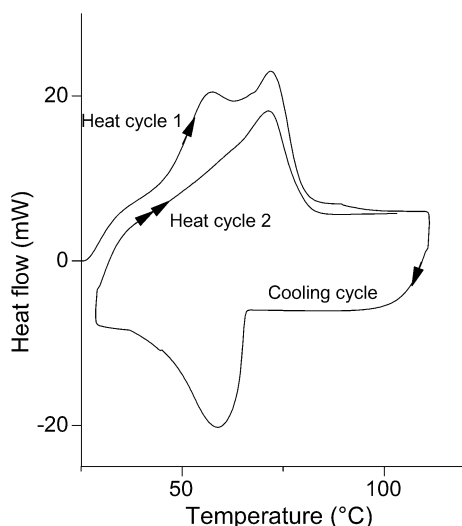


**Figure 6** DSC thermogram showing a heat-cool-heat cycle of PVP/TA fibres formed at  $8000 \text{ r min}^{-1}$  in the coarse spinneret.

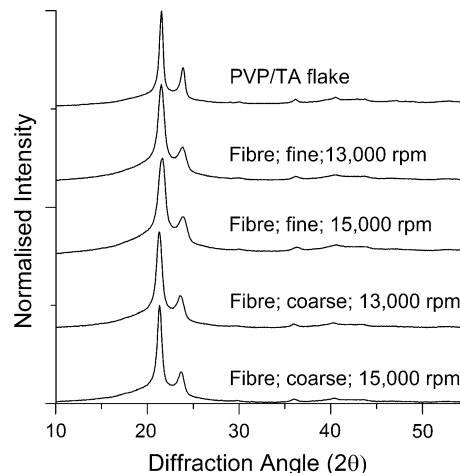


**Figure 7** Selected XRD plots of PVP/TA flake and fibres.

peaks superimposed onto a broad and weak halo that stretches from  $10^\circ$  to  $30^\circ$   $2\theta$ . This broad shoulder is indicative of an amorphous region [31] and it has been demonstrated previously that homogenous PVP exhibits low levels of order in XRD analyses indicating that PVP is entirely amorphous [32, 33]. However, the distinct peaks evident in the XRD patterns for PVP/TA fibres are a strong indicator of long range order and therefore semi-crystallinity. The PVP/TA diffraction pattern has peaks at  $21.6^\circ$ ,  $24.0^\circ$ , and  $36.4^\circ$   $2\theta$  along with additional secondary peaks between  $25^\circ$  and  $40^\circ$   $2\theta$ . The peak locations and diffraction pattern shape are very similar to that of linear and branched polyethylene [34]. Polyethylene forms an orthorhombic crystal with peaks found around  $21.4^\circ$ ,  $24.2^\circ$ , and  $36.5^\circ$   $2\theta$  [35, 36].

It is proposed that PVP/TA forms branched chain crystals where the  $C_{30}$  side chains falls and in crystallographic register with local  $C_{30}$  elements whilst the PVP backbone remains in an amorphous state. The crystallisation of a graft chain on an amorphous backbone is known as interdigitating packing [37]. Deviations in backbone chain registration and variations in chain length would allow for a single copolymer brush to enter both crystalline and amorphous regions and would incorporate further defects and disorder into the crystal system. Previous research has indicated that graft side chains will only crystallise at sufficient distance away from the backbone; this will further limit the size of the crystal formed by the  $C_{30}$  chains in at least one dimension [38, 39]. A simple model of this interaction is given in Fig. 8.

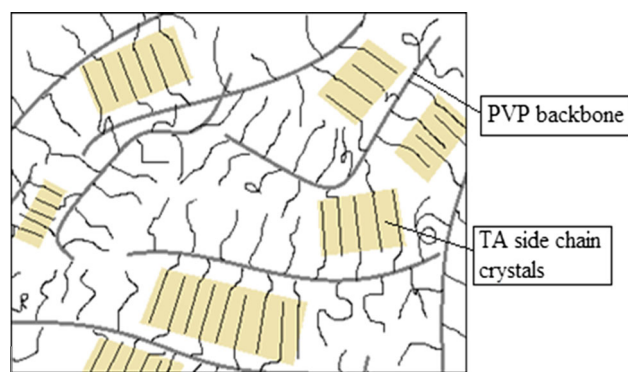


**Figure 8** Schematic model for crystallisation of graft copolymers [37–39].

Based on this structure, there is a possible link between the laterally crystalline structure and the propensity for PVP/TA fibres to undergo brittle fracture. The net orientation of the brush polymer is proposed to be along the length of the fibre and the crystalline elements roughly perpendicular in net orientation. Therefore due to the relatively small dimensions of the crystals, the microfibrils will be capable of slipping more easily relative to chain folding high polymers [40]. This could explain the brittle tensile fractures observed in the SEM micrographs of the fibres. It is hypothesised that these lateral crystals do not contribute to the tensile strength and elasticity associated with crystallised regions in long linear chains [41].

### Adsorbent behaviour of PVP/TA fibres

Having successfully produced PVP/TA fibres for the first time it was deemed useful to determine their feasibility as a fibrous sorption material and their

relative performance against activated carbon. The UV–Vis adsorption values for the filtered solutions were converted into dye concentrations at equilibrium ( $C_e$ ) at each dye bath concentration ( $C_0$ ), using a calibration curve for the disperse dye, Dianix Blue AC-E, in 50:50 acetone. The adsorption at equilibrium ( $Q_e$ ) for the PVP/TA fibres was calculated using  $Q_e = (C_0 - C_e) \frac{V}{m}$  where  $V$  is the volume of solution and  $m$  is the mass of adsorbent.

Table 2 provides the summary of the adsorption at equilibrium figures at each dye concentration along with the degree of removal, calculated using:  $\text{Removal}(\%) = (C_0 - C_e)/C_0 \times 100$ . As indicated the PVP/TA fibres effectively adsorbed the disperse dye molecule, with removal rates of up to 97.1 %, based on an original dye concentration of  $25 \text{ mg dm}^{-3}$ , with an adsorption at equilibrium as high as  $35.4 \text{ mg g}^{-1}$ .

Comparison of the adsorption data, relative to granular activated carbon, indicated that the activated carbon had comparable adsorption of the disperse dye to the PVP/TA fibres but overall had a lower capacity for adsorption with a  $Q_e$  of  $30.0 \text{ mg g}^{-1}$ . The isothermal plots for PVP/TA fibres and activated carbon show that the empirical data are well represented by the Langmuir isothermal model, Fig. 9. The Langmuir model stipulates that adsorption occurs as a single monolayer limited to a finite number of dye sites. Therefore, the isothermal adsorption of disperse dyes on these materials is related to the surface area as this will determine the number of adsorption sites available.

Activated carbon is known for its high surface area due to a fine pore structure, enabling relatively high capture of particulate such as dyes on the surface.

**Table 2** Proportion of disperse dye removed by PVP/TA fibres and activated carbon and amount of dye adsorbed onto the adsorbent fibres and carbon

	Initial dye bath concentration, $C_0$ ( $\text{mg dm}^{-3}$ )					
	25	50	100	150	200	300
<b>Dye/fibre parameters</b>						
Equilibrium concentration $C_e$ ( $\text{mg dm}^{-3}$ )	0.7	8.4	24.7	38.5	61.3	122.8
Dye removal from solution (%)	97.1	83.2	75.3	74.3	70.4	59.1
Adsorption at equilibrium $Q_e$ ( $\text{mg g}^{-1}$ )	4.9	8.3	15.1	22.3	27.7	35.4
<b>Dye/activated carbon parameters</b>						
Equilibrium concentration, $C_e$ ( $\text{mg dm}^{-3}$ )	1.0	5.9	21.5	40.2	73.4	150.4
Dye removal from Solution, (%)	95.9	88.3	78.5	73.2	63.3	49.9
Adsorption at equilibrium, $Q_e$ ( $\text{mg g}^{-1}$ )	4.8	8.8	15.7	22.0	25.3	30.0

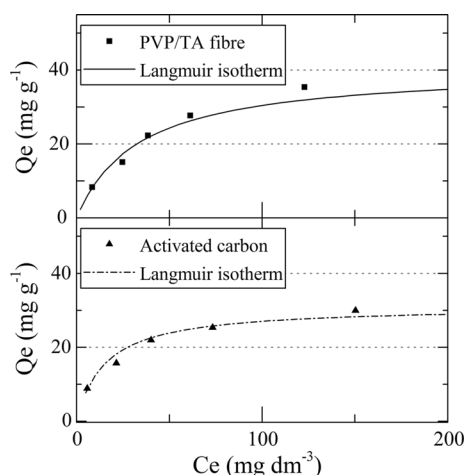


**Figure 9** Recorded data and calculated Langmuir isothermal curves for PVP/TA fibres and activated carbon.

Numerous chemical bonding mechanisms can exist between a surface and a disperse dyes in aqueous media [42]. The literature shows that the adsorption of disperse dyes and other hydrophobic/insoluble compounds is linked to the prevalence of hydrophobic sites on the surface of the material [21, 43]. It is proposed that the adsorption of non-ionic disperse dyes onto such materials occurs through a weak chemical bond such as the non-polar bonding of hydrophobic materials [44, 45]. This “hydrophobic bonding” of non-polar materials in aqueous environments is shown to be unusually strong as it is a combination of interface bonding between the adsorbent and adsorbate and the mutual phobicity for water and other polar aqueous liquids [46–48]. Once two hydrophobic species are brought together, the energy required to dissociate the elements is a function of the energy required to disrupt the hydrogen bonding of the surrounding water molecules, creating a bonding phenomenon that is long range and much stronger than the ionic and electrostatic interaction between the two molecules [46, 47]. The Langmuir model assumes that there is a finite number of ‘active sites’ onto which adsorption can occur. For reactive dyeing, these sites can be related the number of functional groups at the surface of the polymer; for disperse dyeing, onto hydrophobic materials these ‘active sites’ may be regions where hydrophobic bonds are most likely to occur. The triacontene-grafted

chains on the PVP polymer backbone provide the hydrophobic adsorption sites for the PVP/TA fibre. The hydrophilic PVP is masked by the graft chains, creating an entirely hydrophobic surface. In contrast for activated carbon, there are a mixture of hydrophobic and hydrophilic regions, with disperse dyes being captured at hydrophobic regions [49]. As the interaction between PVP/TA and the dye molecules relies on mutual hydrophobicity and does not require elevated temperatures or secondary salts, there is potential to use such a material to collect not only dyes but other material such as hydrocarbons and fatty soils in either a laundry or industrial setting.

## Conclusions

Polyvinylpyrrolidone/triacontene was successfully melt spun into ultrafine fibres through melt centrifugal spinning. Increasing the rotational speed reduced the average fibre diameter with typically the fibre average diameters observed being 1–2  $\mu\text{m}$ , although some individual fibres were observed as fine as 0.2  $\mu\text{m}$ . The fibres were found to be highly brittle, and examples of brittle elastic fracture were observed through SEM analysis of the fibres. DSC and XRD analyses suggest that this brittleness was linked to the graft chain crystallisation where the PVP/TA was in the form of a radial brush copolymer which forms a semi-crystalline structure where the triacontene branches interlock and form small lateral crystals around an amorphous backbone. The radial triacontene branches also impart hydrophobicity and “mask” the hydrophilic nature of the PVP backbone.

This hydrophobic behaviour could potentially be useful in adsorption applications and this research assessed the effectiveness of PVP/TA fibres as a dye adsorbent. This was the first time that PVP/TA fibres have been considered as an adsorbent for disperse dyes. The PVP/TA fibres had an adsorption capacity of 35.4  $\text{mg g}^{-1}$  of Dianix Blue A-CE under neutral conditions, exceeding the capacity observed for granular-activated carbon. The hydrophobic nature of the PVP/TA fibres and associated high surface area potentially offers a suitable adsorbent medium for disperse dyes, binding the colorants through non-polar hydrophobic interactions.

## Acknowledgements

The authors would like to thank The Clothworkers' Company for funding the PhD studies of Tom O'Haire.

**Open Access** This article is distributed under the terms of the Creative Commons Attribution 4.0 International License (<http://creativecommons.org/licenses/by/4.0/>), which permits unrestricted use, distribution, and reproduction in any medium, provided you give appropriate credit to the original author(s) and the source, provide a link to the Creative Commons license, and indicate if changes were made.

## References

- [1] Login RB, Barabas ES (1996) Personal care application polymers (acetylene-derived). In: Salamone JC (ed) *Polymeric materials encyclopedia*. CRC Press, Boca Raton
- [2] Brittain WJ, Minko S (2007) A structural definition of polymer brushes. *J Polym Sci Part A* 45(16):3505–3512
- [3] Puccetti G, Fares H (2014) A new approach for evaluating the water resistance of sunscreens on consumers: : tap water vs. salt water vs. chlorine water. *Int J Cosmet Sci* 36(3):284–290
- [4] Brugnara M, Degasperis E, Volpe CD, Maniglio D, Penati A, Siboni S, Toniolo L, Poli T, Invernizzi S, Castelvetro V (2004) The application of the contact angle in monument protection: new materials and methods. *Colloid Surf A* 241(1–3):299–312
- [5] Liu KC, Heliouff M, Rerek M, Davis LJ, Grenner DE, Waldorf-Geber A, Koppel R (1997) Sunscreen concentrate. United States Patent 5,916,544
- [6] Snyder F, Reinhart G, DiGirolamo D (1995) Cosmetic compositions for lengthening, coloring and curling eyelashes. United States Patent 5,389,363
- [7] Grinwald Y, Bar-Haim G, Berson Y (2015) Positively charged ink composition. United States Patent 8,927,635
- [8] Yu DG, White K, Yang JH, Wang X, Qian W, Li Y (2012) PVP nanofibers prepared using co-axial electrospinning with salt solution as sheath fluid. *Mater Lett* 67(1):78–80
- [9] Wahyudiono Machmudah S, Murakami K, Okubayashi S, Goto M (2013) Generation of PVP fibers by electrospinning in one-step process under high-pressure CO<sub>2</sub>. *Int J Ind Chem* 4(1):1–6
- [10] Chen H, Xu H, Sun J, Liu C, Yang B (2015) Effective method for high-throughput manufacturing of ultrafine fibres via needleless centrifugal spinning. *Micro Nano Lett* 10(2):81–84
- [11] Liu SL, Long YZ, Zhang ZH, Zhang HD, Sun B, Zhang JC, Han WP (2013) Assembly of oriented ultrafine polymer fibers by centrifugal electrospinning. *J Nanomater* 2013:9
- [12] McCann JT, Marquez M, Xia Y (2006) Melt coaxial electrospinning: a versatile method for the encapsulation of solid materials and fabrication of phase change nanofibers. *Nano Lett* 6(12):2868–2872
- [13] O'Haire T, Rigout M, Russell S, Carr C (2014) Influence of nanotube dispersion and spinning conditions on nanofibre nanocomposites of polypropylene and multi-walled carbon nanotubes produced through Forcespinning™. *J Thermoplast Compos Mater* 27(2):205–214
- [14] Sarkar K, Gomez C, Zambrano S, Ramirez M, de Hoyos E, Vasquez H, Lozano K (2010) Electrospinning to Forcespinning™. *Mater Today* 13(11):12–14
- [15] McEachin Z, Lozano K (2011) Production and characterization of polycaprolactone nanofibres via Forcespinning™ technology. *J Appl Polym Sci* 126:473–479
- [16] Bandla S, Winarski R, Hanan J (2013) Nanotomography of polymer nanocomposite nanofibers. In: Jin H, Sciammarella C, Furlong C, Yoshida S (eds) *Imaging methods for novel materials and challenging applications*, vol 3. Springer, New York, pp 193–198
- [17] Gramley K (2012) Forcespinning ceramic nanofibres. *Adv Ceram Rep* 2012(2):6–7
- [18] Cavazzuti R, Mattox BK, Swanborough M (2002) Mixture of wax, ester and fatty alcohol. United States Patent 6,444,212
- [19] Christie R (2014) *Colour chemistry*. Royal Society of Chemistry, London
- [20] Carneiro PA, Umbuzeiro GA, Oliveira DP, Zanoni MVB (2010) Assessment of water contamination caused by a mutagenic textile effluent/dyehouse effluent bearing disperse dyes. *J Hazard Mater* 174(1):694–699
- [21] Rai PB, Banerjee SS, Jayaram RV (2007) Removal of disperse dyes from aqueous solution using sawdust and BDTDA/sawdust. *J Dispers Sci Technol* 28(7):1066–1071
- [22] Eschway H, Hackler L, Hartmann L, Kauschke M, Kumpel T, Kunkel HA, Nahe T, Ruzek I (1990) Absorbent body of nonwoven material and a method for the production thereof. United States Patent, 4,902,559
- [23] Allen S, McKay G, Porter J (2004) Adsorption isotherm models for basic dye adsorption by peat in single and binary component systems. *J Colloid Interface Sci* 280(2):322–333
- [24] El-Geundi MS (1991) Colour removal from textile effluents by adsorption techniques. *Water Res* 25(3):271–273

- [25] O'Haire T (2015) The production of ultrafine fibres using variations of the centrifugal spinning technique. PhD Dissertation, University of Leeds
- [26] Ellison CJ, Phatak A, Giles DW, Macosko CW, Bates FS (2007) Melt blown nanofibers: fiber diameter distributions and onset of fiber breakup. *Polymer* 48(11):3306–3316
- [27] Hearle JW, Lomas B, Cooke WD (1998) Atlas of fibre fracture and damage to textiles. Elsevier, London
- [28] Hearle JW (2002) Forms of fibre fracture. In: Elices M, Llorca J (eds) Fiber fracture. Elsevier, Oxford, pp 57–71
- [29] Barham P, Hill M, Keller A, Rosney CD (1988) Phase separation in polyethylene melts. *J Mater Sci Lett* 7(12):1271–1275
- [30] Blundell D (1987) On the interpretation of multiple melting peaks in poly (ether ether ketone). *Polymer* 28(13):2248–2251
- [31] Camini R, Pandolfi L, Ballirano P (2000) Structure of polyethylene from X-ray powder diffraction: influence of the amorphous fraction on data analysis. *J Macromol Sci B* 39(4):481–492
- [32] Razzak MT, Dewi S, Lely H, Taty E (1999) The characterization of dressing component materials and radiation formation of PVA–PVP hydrogel. *Radiat Phys Chem* 55(2):153–165
- [33] Sethia S, Squillante E (2004) Solid dispersion of carbamazepine in PVP K30 by conventional solvent evaporation and supercritical methods. *Int J Pharm* 272(1–2):1–10
- [34] Ueno N, Seki K, Sugita K, Inokuchi H (1991) Nature of the temperature dependence of conduction bands in polyethylene. *Phys Rev B* 43(3):2384–2390
- [35] Smith P, Lemstra P (1980) Ultra-high-strength polyethylene filaments by solution spinning/drawing. *J Mater Sci* 15(2):505–514 doi:10.1007/BF00551705
- [36] Zheng L, Waddon AJ, Farris RJ, Coughlin EB (2002) X-ray characterizations of polyethylene polyhedral oligomeric silsesquioxane copolymers. *Macromolecules* 35(6):2375–2379
- [37] Neugebauer D, Theis M, Pakula T, Wegner G, Matyjaszewski K (2006) Densely heterografted brush macromolecules with crystallizable grafts: synthesis and bulk properties. *Macromolecules* 39(2):584–593
- [38] Schouten AJ, Wegner G (1991) Langmuir–Blodgett mono- and multilayers of preformed poly (octadecyl methacrylate)s, 1. Surface-area isotherms of atactic and isotactic poly(octadecyl methacrylate)s and transfer into multilayers. *Die Makromol Chem* 192(10):2203–2213
- [39] Arndt T, Schouten AJ, Schmidt GF, Wegner G (1991) Langmuir–Blodgett mono- and multilayers of preformed poly (octadecyl methacrylate)s, 2. Structural studies by IR spectroscopy and small-angle X-ray scattering. *Die Makromol Chem* 192(10):2215–2229
- [40] Peterlin A (1972) Morphology and properties of crystalline polymers with fiber structure. *Text Res J* 42(1):20–30
- [41] Sui K, Liang H, Zhao X, Ma Y, Zhang Y, Xia Y (2012) Synthesis of amphiphilic poly(ethylene oxide-co-glycidol)-graft-polyacrylonitrile brush copolymers and their self-assembly in aqueous media. *Macromol Chem Phys* 213(16):1717–1724
- [42] Giles CH (1961) Studies in adsorption, part XIV: the mechanism of adsorption of dispersed dyes by cellulose acetates and other hydrophobic fibers. *Tex Res J* 31(2):141–151
- [43] Dąbrowski A, Podkościelny P, Hubicki Z, Barczak M (2005) Adsorption of phenolic compounds by activated carbon—a critical review. *Chemosphere* 58(8):1049–1070
- [44] Derbyshire AN, Peters RH (1955) An explanation of dyeing mechanisms in terms of non-polar bonding. *J Soc Dyers Colour* 71(9):530–536
- [45] Moreno-Castilla C (2004) Adsorption of organic molecules from aqueous solutions on carbon materials. *Carbon* 42(1):83–94
- [46] Israelachvili J, Pashley R (1982) The hydrophobic interaction is long range, decaying exponentially with distance. *Nature* 300(5890):341–342
- [47] Franks F (2013) Water: a comprehensive treatise: volume 4: aqueous solutions of amphiphiles and macromolecules. Springer, London
- [48] Pashley R, McGuiggan P, Ninham B, Evans D (1985) Attractive forces between uncharged hydrophobic surfaces: direct measurements in aqueous solution. *Science* 229(4718):1088–1089
- [49] Groszek A, Partyka S (1993) Measurements of hydrophobic and hydrophilic surface sites by flow microcalorimetry. *Langmuir* 9(10):2721–2725